Simulation of SAW-Driven Microparticle Acoustophoresis Using COMSOL Multiphysics® Software

N. Nama[1], R. Barnkob[2], C. J. Kähler[2], T. J. Huang[1], F. Costanzo[1]

[1]Department of Engineering Science and Mechanics, Pennsylvania State University, PA, USA
[2]Institute of Fluid Mechanics and Aerodynamics, Bundeswehr University Munich, Neubiberg, Germany

Abstract

Introduction - The ability to precisely manipulate fluid and particles at microscales is one of the essential requirements for various lab-on-a-chip applications such as drug diagnostics, chemical synthesis etc.[1] Recently, the nonlinear interaction of surface acoustic waves (SAW) with fluid at microscales has been utilized to achieve this aim. When surface acoustic waves interact with fluid inside a microchannel, they radiate acoustic energy into the fluid. This sets the fluid into motion (referred as acoustic streaming) and also results into an acoustic radiation force on the particles immersed in the fluid. In this work, we present a perturbation approach based numerical model to study SAW-driven acoustophoretic motion of particles in microchannels under the influence of both the acoustic streaming induced drag force as well as the acoustic radiation force.

Use of COMSOL Multiphysics® - We model the fluid using the compressible Navier-Stokes equations in COMSOL Multiphysics® software. To circumvent the wide length and time scales associated with the typical SAW devices, we employed a perturbation approach resulting in first- and second-order equations (Figure 2), which are then successively solved using appropriate boundary conditions (Figure 1). To resolve the boundary layers near the mesh, the mesh was heavily refined near the walls (Figure 2). Since the second-order equations include a body force arising from the first-order terms, these equations can be solved successively using both the Weak Form PDE physics interface and the Laminar Flow interface.

Results - Figure 3 shows the acoustic fields (first-order pressure, p1 and velocity, v1) inside the microchannel, which are characterized by a standing wave along the horizontal direction, but a traveling wave is observed in the vertical direction moving from the bottom to the top wall, as indicated by the arrows. Figure 3 also shows the second-order acoustic streaming velocity, v2, indicating four streaming vortices along the channel width. Figure 4 shows the acoustophoretic motion of particles under the influence of acoustic radiation force and acoustic streaming for three different particle diameters: (b) 1 µm; (c) 5 µm, and (d) 20 µm. It can be seen that the motion of smaller particles is completely dominated by the streaming-induced drag force and the small particles follow the acoustic streaming patterns shown in Figure 3. However, for increasing

particle sizes, the radiation force becomes significant and for large particles, the motion is completely dominated by the acoustic radiation force pushing the particle to the pressure node along the center of the channel.

Conclusion - In conclusion, we present a numerical model for SAW devices and identify the acoustic fields and the resulting particle motion inside the microchannel. We investigated a range of particle diameters to study the transition from streaming-drag-dominated acoustophoresis to radiation-force-dominated acoustophoresis. Our model would be useful for the optimization of SAW-based devices for various lab-on-a-chip applications.

Reference

1. X. Ding et. al., Lab on a Chip, Vol. 13, 3626-3649 (2013).

Figures used in the abstract

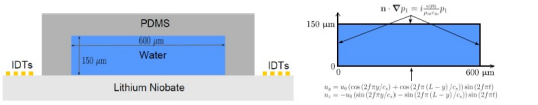

Figure 1: (a) Cross-sectional sketch of the SAW device with a microfluidic PDMS channel of width $w = 600$ μm and height $h = 150$ μm. (b) Two-dimensional computational domain subject to impedance boundary conditions (water/PDMS interfaces) and actuation condition (water/substrate inteface).

Figure 1

First-Order Equations

$$\frac{\partial \rho_1}{\partial t} + \rho_0(\boldsymbol{\nabla}\cdot\boldsymbol{v}_1) = 0,$$

$$\rho_0\frac{\partial \boldsymbol{v}_1}{\partial t} = -\boldsymbol{\nabla}p_1 + \mu\nabla^2\boldsymbol{v}_1 + (\mu_b + \tfrac{1}{3}\mu)\boldsymbol{\nabla}(\boldsymbol{\nabla}\cdot\boldsymbol{v}_1).$$

Second-Order Equations

$$\left\langle\frac{\partial \rho_2}{\partial t}\right\rangle + \rho_0\boldsymbol{\nabla}\cdot\langle\boldsymbol{v}_2\rangle = -\boldsymbol{\nabla}\cdot\langle\rho_1\boldsymbol{v}_1\rangle,$$

$$\rho_0\left\langle\frac{\partial \boldsymbol{v}_2}{\partial t}\right\rangle + \left\langle\rho_1\frac{\partial \boldsymbol{v}_1}{\partial t}\right\rangle + \rho_0\langle\boldsymbol{v}_1\cdot\boldsymbol{\nabla}\boldsymbol{v}_1\rangle$$
$$= -\boldsymbol{\nabla}\langle p_2\rangle + \mu\nabla^2\langle\boldsymbol{v}_2\rangle + (\mu_b + \tfrac{1}{3}\mu)\boldsymbol{\nabla}(\boldsymbol{\nabla}\cdot\langle\boldsymbol{v}_2\rangle),$$

Figure 2: Governing Equations

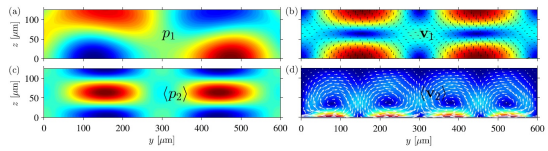

Figure 2: (a) First-order pressure p_1 (from blue -5.7 kPa to red 5.7 kPa). (b) First-order velocity v_1 (magnitude from blue 0 to red 8.4 mm/s). (c) Second-order time-averaged pressure $\langle p_2 \rangle$ (from blue -16.4 mPa to red 18.8 mPa). (d) Second-order time-average velocity $\langle v_2 \rangle$ (magnitude from blue 0 to red 2.5 μm/s).

Figure 3

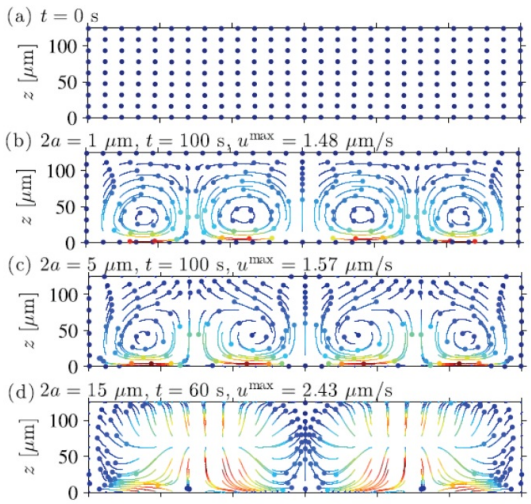

Fig. 4 (a) Starting position of particles distributed uniformly within the microchannel. (b)-(d) show the plots of particle trajectories for (b) 1 μm particles during 100s, (c) 5 μm particles during 100s, and (d) 1 μm particles during 60s.

Figure 4